Generating Interchangeable 20° Spur Gear Sets with Circular Fillets to Increase Load Carrying Capacity

Christos A. Spitas and Vasilis A. Spitas

Optimal Gears of V0 Design
$z_1 = 15$, $z_2 = 50$
Pinion
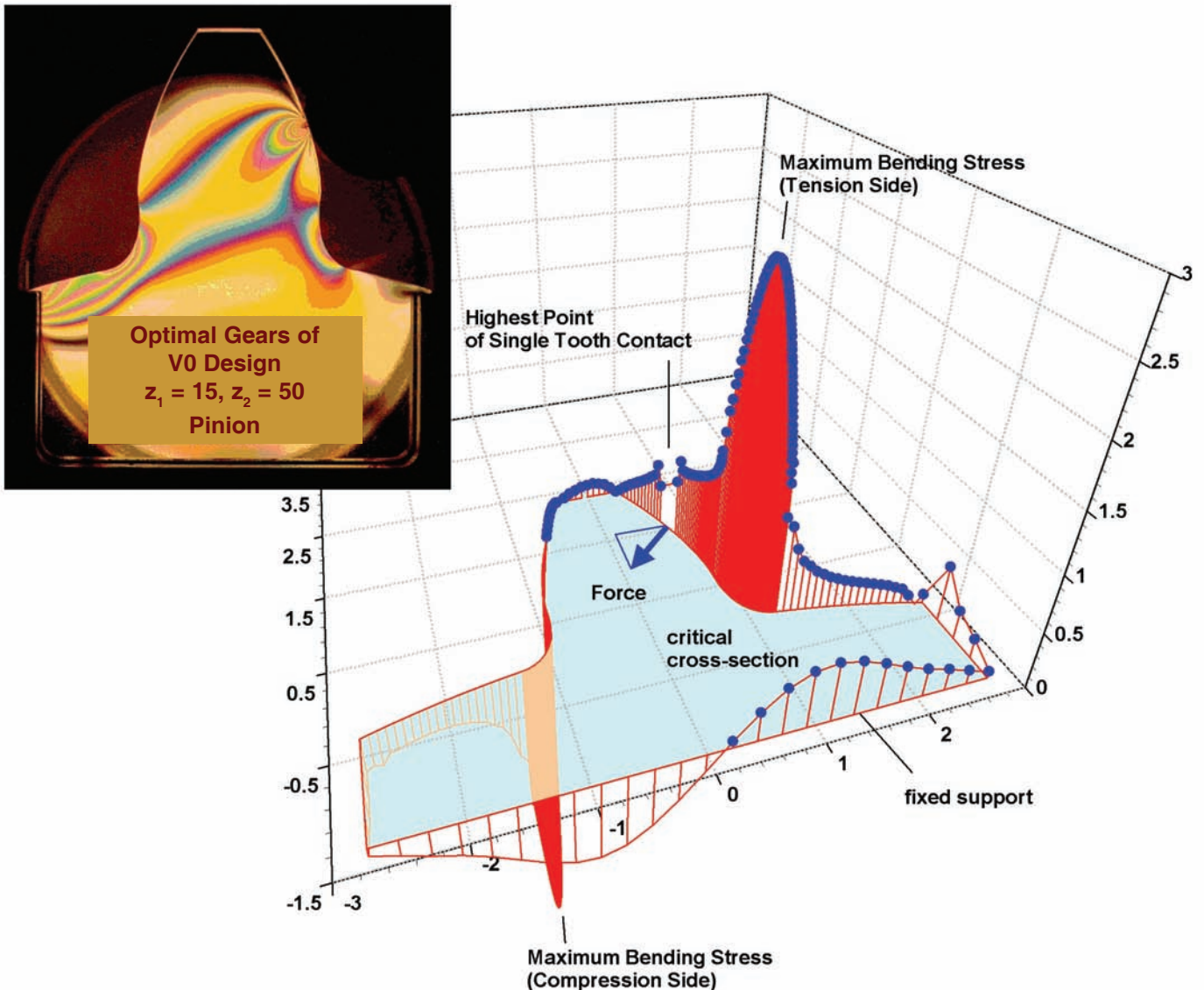
Management Summary

This article presents a new spur gear 20° design that works interchangeably with the standard 20° system and achieves increased tooth bending strength and hence load carrying capacity. In this design, a circular fillet replaces the normal trochoidal fillet, yielding larger cross-sections at the tooth root and lower stress concentration. The actual working tooth profiles remain unaffected. To verify this design, a series of numerical simulations was carried out using the boundary element method (BEM), and the results were confirmed with subsequent laboratory testing.

Introduction

The vast majority of gear applications use the standard 20° involute system because of its good combination of bending and surface pressure strength, involute insensitivity to errors in center distance and relative ease of manufacturing. Most gears are produced by hobbing or other generation-type processes, where a straight-tooth rack or equivalent tool produces the involute working gear tooth surface as well as a trochoidal root fillet.

Despite the benefits of this system, it is generally felt that a higher bending strength and hence load carrying capacity should be obtained. This is especially true with small numbers of teeth (less than 14 or 17 depending on the tip radius of the hob), where the standard involute teeth are susceptible to undercutting. This is a situation where the tip of the cutter removes material from the involute profile in a secondary cutting action. The resulting teeth have smaller thicknesses near their roots, where the critical section is usually located (Refs. 1–2), and this severely hampers load carrying capacity.

Up to now, a number of different gear tooth designs have been proposed aiming to address this problem (Refs. 3–4), but the most commonly employed method is that of positive profile shifting (Refs. 5–8), resulting in teeth with no undercutting, with enhanced fatigue characteristics and with changes in the nominal center distance of the gear pair. Other solutions of a hybrid-type have been proposed by Litvin et al. (Ref. 9) and Tsai and Tsai (Ref. 10). These designs typically rely on sturdier tooth forms, which often present unfavorable side effects, such as 1.) increase of average sliding velocity, 2.) non-interchangeability with the standard 20° tooth systems either due to shifting or due to non-involute shapes, 3.) lower pitting and scoring resistance, 4.) lower contact ratio resulting in more noise and vibration during operation (Ref. 2), and 5.) increased complexity and hence manufacturing costs. Clearly, any viable alternative to the standard system should, as a matter of course, address these issues effectively.

In this context, the present article takes into account a number of gear tooth design concepts developed by the authors (Ref. 11) in order to produce gear teeth with load carrying capacity increased up to 130% of the standard designs whilst keeping the rest of the gear pair working conditions unaffected. The resulting interchangeable spur gear tooth systems are generated by simple hobbing tool geometry, using standard cutting machines and procedures. The feature that increases the load carrying capacity in the gear teeth is the substitution of the standard trochoidal fillet produced with the standard circular-filleted hob teeth with a circular arc fillet generated with modified hob tip geometry.

The work reported in this article comprises the full generation, simulation and verification cycle of the new design encompassing: 1.) design of hob cutter fillet geometry, 2.) simulation of generation process, 3.) strength evaluation and comparison with standard gears using BEM, 4.) manufacture of gear tooth samples in the laboratory workshop, and 5.) static load carrying capacity testing of generated gears by measuring maximum fillet stress using photoelasticity.

The test results show agreement with the anticipated values, and the circular fillet design is proven to give consistently better results than the standard trochoidal fillet. The beneficial effect is more pronounced with tooth numbers fewer than 40. In addition, the usual undercutting restrictions are shown to no longer apply to circular fillet teeth cut with the present method, so that pinions of as few as nine teeth can be produced, possessing a load carrying capacity of more than three times that of standard undercut teeth.

Geometrical Analysis

As a first step, the gear model is non-dimensionalized with respect to the gear module (Ref. 11), so that a wider generality of the results can be achieved. The process follows.

Consider a pair of spur gears in mesh. Both gears should have the same nominal pressure angle α_o and the same module m in order to be able to mesh properly. It is also possible that these gears have addendum modifications x_1 and x_2, respectively, and therefore their pitch thickness is given by the following relationship:

$$s_{oi} = c_{si}\pi m + 2x_i \tan\alpha_o m = s_{oiu}m \qquad (1)$$

where c_{si} is the thickness coefficient of gear i, (i = 1, 2), which in the general case is $c_{s1} \neq 0.5 \neq c_{s2}$, while s_{oiu} is the pitch thickness of the corresponding non-dimensional gear for which the module (m) and the face width (b) are both equal to unity.

In the absence of errors, the center distance and working pitch circle radius expressions are:

$$a_{12} = \frac{z_1 + z_2}{2}m + (x_1 + x_2)m = a_{12u}m \qquad (2)$$

$$r_{bi} = \frac{z_i}{z_1 + z_2}a_{12u}m = r_{biu}m \qquad (3)$$

Furthermore, Spitas (Ref. 12) has shown that the radius defining the position of the highest point of single tooth contact (HPSTC) on gear 1 can be expressed as:

$$r_{B'u} = \frac{r_{B'}}{m} = \sqrt{r_{k1u}^2 + (\varepsilon - 1)t_{gu}\left[(\varepsilon - 1)t_{gu} - 2\sqrt{r_{k1u}^2 - r_{g1u}^2}\right]} \qquad (4)$$

The above equations show that it is possible to describe the governing relationships in the gear pair in a more generalized way, by non-dimensionalizing in terms of the module. This reduces the needed variables, as the interaction of a given

Dr. Christos A. Spitas *is a professor at the Technical University of Crete, in its department of production engineering and management. He holds a doctorate in mechanical engineering and specializes in gears. Besides teaching, he performs research on gear geometrical/kinematical modelling, profile errors, dynamics, wear and heat transfer. He's written 45 scientific papers in the fields of gearing, materials testing and heat transfer.*

Dr. Vasilis A. Spitas *is a professor at the Technical University of Crete, in its general science department and its applied mechanics laboratory. He holds a doctorate in mechanical engineering, with a specialization in gears. Also, he performs research on gear generation, fillet strength, crack propagation, numerical analysis (FEM, BEM), experimental analysis (photoelasticity, caustics), and design optimization. He's author of more than 50 scientific papers, as well as 20 technical reports in the fields of gearing, materials testing, experimental and computational mechanics and smart materials.*

gear with any mating gear need only consider the contact ratio instead of the full set of the mating gear attributes. Also, the use of non-dimensional teeth allows every geometrical feature f_i on the transverse section of a full-scale gear tooth to be connected with the corresponding feature f_u of the transverse section of the non-dimensional gear tooth through the equation:

$$f = f_u m \qquad (5)$$

Stresses can also be calculated in non-dimensional teeth $\sigma_u(z, x, c_s, \varepsilon)$ with unit loading $P_{Nu} = 1$ and be related to the actual stress σ using the following equation:

$$\sigma = \sigma_u \frac{P_N}{b\,m} \qquad (6)$$

as suggested by Rogers (Ref. 8) and Townsend (Ref. 1).

Having defined the non-dimensional form of the problem, the novel circular fillet tooth geometry is defined through the following procedure.
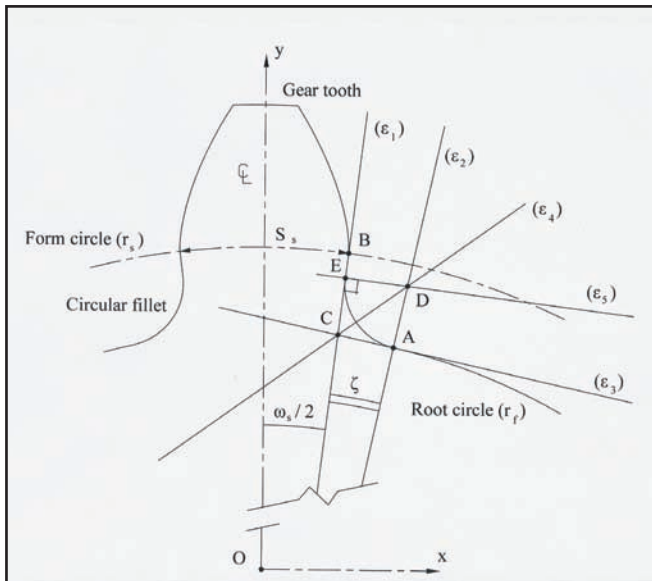
Figure 1—The geometry of the circular fillet.
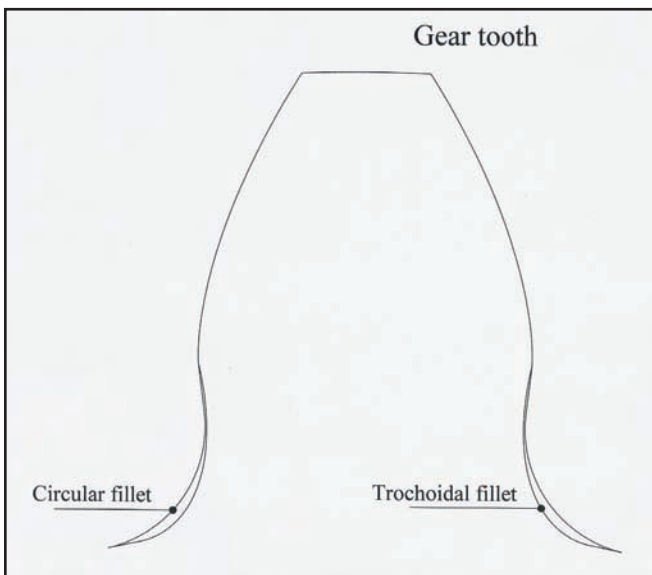
Figure 2—Superposition of circular fillet on a standard tooth.

Consider the involute spur gear tooth of circular fillet illustrated in Figure 1, where point 0 is the center of the gear, axis 0y is the axis of symmetry of the tooth and point B is the point where the involute profile starts.

Point A is the point of tangency of the circular fillet with the root circle r_f. Point D lying on $\varepsilon_2 \equiv$ OA represents the center of the circular fillet. Line ε_3 is tangent to the root circle at A and intersects with line ε_1 at C. The fillet is tangent to the line ε_1 at point E. Since it is always $r_s > r_f$ (Ref. 1), the proposed circular fillet can be implemented without exceptions on all spur gears regardless of the number of teeth or other manufacturing parameters. A comparison of the geometrical shapes of a tooth with a circular fillet and of one with a standard fillet is presented in Figure 2.

For the geometrical modelling, only non-dimensional teeth are examined, i.e. teeth with unit module (m) and face width (b). In non-dimensional teeth, the pitch radius and the pitch thickness are calculated:

$$r_o = \frac{z}{2} \quad \text{and} \quad S_{ov} = \pi c_s + 2x \tan \alpha_o \qquad (7)$$

$$S_s = r_s \left[\frac{S_{ov}}{r_o} + 2(\varphi_o - \varphi_s) \right] \qquad (8)$$

where:
$\varphi_s = \tan \alpha_s - \alpha_s$ is the involute function on circle r_s and
$\alpha_s = \cos^{-1}(r_g/r_s)$ is the pressure angle on circle r_s

Angle $\omega_s/2$ that corresponds to the arc $S_s/2$ (Fig. 1) is given by the equation:

$$\omega_s/2 = \frac{S_s/2}{r_s} = \Omega_s \qquad (9)$$

Angle ζ (Fig. 1) takes values between 0 and ζ_{max} so that:

$$\zeta_{max} = \frac{\pi}{z} - \Omega_s \qquad (10)$$

The coordinates of points A and B are:

$$x_A = r_f \sin(\zeta + \Omega_s), \quad y_A = r_f \cos(\zeta + \Omega_s) \qquad (11)$$

$$x_B = r_f \sin \Omega_s, \quad y_B = r_f \cos \Omega_s \qquad (12)$$

The defining equations of lines ε_1 and ε_2 are, respectively:

$$(\varepsilon_1): y = \frac{1}{\tan \Omega_s} x, \quad (\varepsilon_2): y = \frac{1}{\tan(\zeta + \Omega_s)} x \qquad (13)$$

Since ε_3 is perpendicular to ε_2 and ε_3 passes through point A(x_A, y_A) its defining equation is:

$$y = -\tan(\zeta + \Omega_s)x + \frac{r_f}{\cos(\zeta + \Omega_s)} \qquad (14)$$

Point C(x_C, y_C) is the intersection of ε_1 and ε_3, and therefore its coordinates should verify Equation 13 and hence:

$$x_C = r_f \frac{\tan \Omega_s}{\sin(\zeta + \Omega_s)\tan \Omega_s + \cos(\zeta + \Omega_s)}, \quad y_C = \frac{x_C}{\tan \Omega_s} \qquad (15)$$

Angle B$\hat{C}$A is calculated as:

$$\hat{B}CA = \left(\frac{\pi}{2} - \Omega_s\right) + \zeta + \Omega_s = \frac{\pi}{2} + \zeta \quad (16)$$

Line ε_4 bisects the previous angle $\hat{B}CA$, so its inclination is:

$$\tan\left[\frac{\hat{B}CA}{2} - (\zeta + \Omega_s)\right] = \tan\left(\frac{\pi}{4} - \frac{\zeta}{2} - \Omega_s\right) \quad (17)$$

Point $C(x_C, y_C)$ belongs to ε_4 and thus the defining equation of line ε_4 is derived as:

$$y = \tan\left(\frac{\pi}{4} - \frac{\zeta}{2} - \Omega_s\right)x + r_f \frac{1 - \tan\Omega_s \tan\left(\frac{\pi}{4} - \frac{\zeta}{2} - \Omega_s\right)}{\sin(\zeta + \Omega_s)\tan\Omega_s + \cos(\zeta + \Omega_s)} \quad (18)$$

At this point, two distinct cases are considered. Point E coincides with point B ($E \equiv B$). In this case, ε_5 is perpendicular to ε_1 at point $E \equiv B$, so ε_5 must have an inclination equal to $-\tan\Omega_s$, and since point B belongs to ε_5, its defining equation is:

$$y = -\tan\Omega_s x + \frac{r_s}{\cos\Omega_s} \quad (19)$$

Point $D(x_D, y_D)$ should verify both Equations 13 and 19 and therefore has the following coordinates:

$$x_D = r_s \frac{\tan(\zeta + \Omega_s)}{\cos\Omega_s + \sin\Omega_s \tan(\zeta + \Omega_s)},$$
$$y_D = r_s \frac{1}{\cos\Omega_s + \sin\Omega_s \tan(\zeta + \Omega_s)} \quad (20)$$

According to Figure 1, it is AC = BC, and after substitutions and calculations, we arrive at the equation:

$$\frac{r_f^2 + r_s^2}{2} = \frac{r_s r_f}{\cos\zeta}\left(\sin^2\Omega_s + \cos^2\Omega_s\right) \quad (21)$$

from which the value of ζ is derived as:

$$\zeta = \cos^{-1}\frac{2r_s r_f}{r_s^2 + r_f^2} \quad (22)$$

By defining the non-dimensional parameter $S_i = r_s/r_f > 1$, Equation 22 becomes:

$$\zeta = \cos^{-1}\left(\frac{2S}{1 + S^2}\right) \quad (23)$$

Equation 23 is used for the determination of angle (ζ). Point E lies below point B.

In this case, it is $\zeta \leq \zeta_{max}$, and the center of the circular fillet of the tooth is calculated following the methodology described below:

$$CA = \sqrt{(x_A - x_C)^2 + (y_A - y_C)^2} = CE \quad (24)$$

$$AD = CA \tan\left(\frac{\pi}{4} + \frac{\zeta}{2}\right) \quad (25)$$

The coordinates of points $D(x_D, y_D)$ and $E(x_E, y_E)$ are, respectively:

$$x_D = (r_f + AD)\sin(\zeta + \Omega_s), \quad y_D = (r_f + AD)\cos(\zeta + \Omega_s) \quad (26)$$

$$x_E = (OC + CE)\sin\Omega_s, \quad y_E = (OC + CE)\cos\Omega_s \quad (27)$$
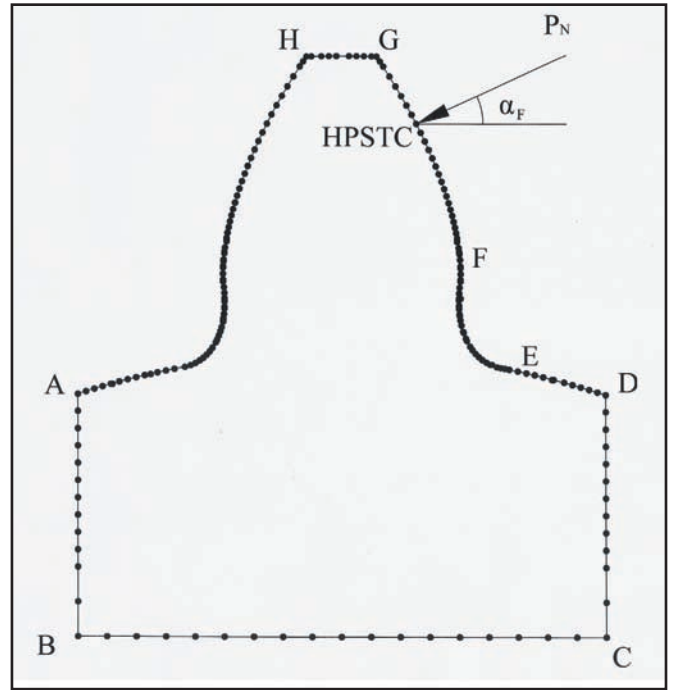
Figure 3—BEM mesh on a tooth model.

The remaining portion of the tooth profile between points B and E is a straight line.

Stress Analysis

The structural analysis of the spur gear tooth model is carried out using the boundary element method with quadratic isoparametric boundary elements. The calculation of the non-dimensional tooth profile and the generation of the mesh are done automatically using specially developed software. A unitary normal load is exerted at the highest point of single tooth contact (HPSTC). The resultant normalized stress is related to the actual stress of the full-scale tooth with Equation 6. The distance of the HPSTC from the center of the gear is calculated in terms of the contact ratio ε and the geometrical characteristics of the gear according to Equation 4.

A typical mesh is presented in Figure 3. The tooth base, ABCD, is discretized in 43 nodes or 21 elements and is considered to be fixed, i.e. the displacements of all nodes are zero.

Portion DE represents the root circle and is discretized in 11 nodes or five elements. Portion EF is the tooth fillet consisting of 72 elements or 144 nodes, portion FG is the involute part of the tooth consisting of 40 elements or 81 nodes and finally portion GH is the tip, discretized in five elements or 11 nodes. All nodes belonging to the tooth profile are considered to be unloaded (horizontal and vertical traction equal to zero) with the exception of the node marked HPSTC, which belongs to the involute part FG and on which the normal load P_N is acting.

The reason that the mesh is denser at the tooth fillet is that the maximum stress is expected to occur in this area, and therefore greater density will ensure increased accuracy of the results (both the position of the critical section and the magnitude of the maximum developed stress).

Manufacture of Test Gear Tooth Specimens

Several test gear tooth specimens with both standard trochoidal as well as circular fillets were produced by precision milling on a CNC machine tool in compliance with the geom-
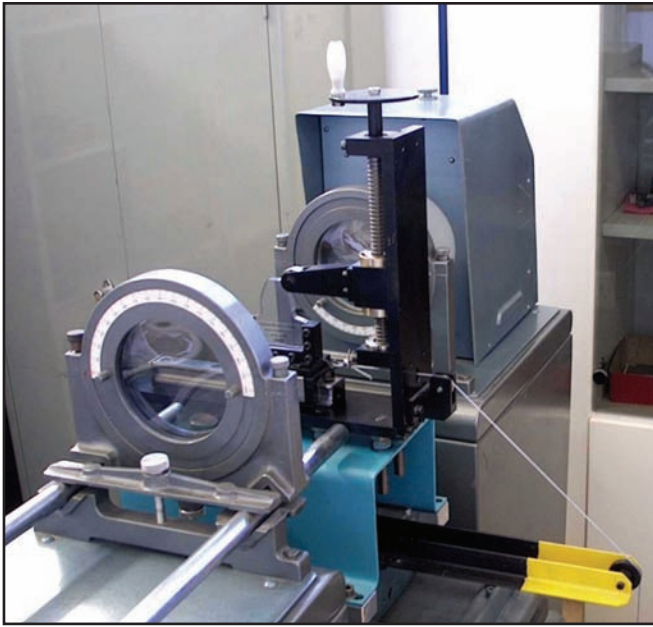
Figure 4—Test rig. Polariscope and loading apparatus with tooth specimen loaded at the tip.

etry of the BEM analysis layout to ensure full comparability of results. The specimens were produced from polycarbonate material suitable for photoelastic investigations. The other fixed parameters are: module = 5 mm, thickness coefficient = 0.5, and profile shift = 0.0

Specimens were produced to correspond to gears with tooth numbers 9, 17, 24, 32 and 40, covering the most basic range of teeth where the circular fillet is expected to yield the most noticeable benefits.

The cutting parameters were selected such that no distortion or residual stress would be present in the specimens. Indeed, all specimens underwent preliminary photoelastic testing in their unloaded state after machining. The residual stresses were negligible. Geometrical survey conducted on a TESA CMM yielded a maximum form deviation of 0.08 mm, which was deemed quite satisfactory given the overall large scale of the models and the required accuracy.

Experimental Verification

A comparative study was carried out between the structural properties of the standard trochoidal-filleted teeth generated by hobbing and the proposed circular-filleted involute teeth. Five distinct cases were examined for unshifted teeth with 9, 17, 24, 32 and 40 teeth, respectively. Results were general regardless of module because of the non-dimensional treatment of the governing equations as explained in the previous analysis.

The test rig used for mounting and loading the tooth specimens for photoelastic measurements is a customized design produced in the Machine Elements Laboratory of the National Technical University of Athens. The rig was mounted on a plane polariscope equipped with mercury and sodium vapor lamps in order to produce the various light wavelengths needed for the measurements. The test rig is presented in Figure 4.

Results and Discussion

In the case of trochoidal-filleted teeth, the N = 9 teeth case presented severe undercutting. The teeth were loaded at their highest point of single tooth contact (HPSTC) and since it has been established that the HPSTC for any given gear pair depends only on the geometrical characteristics of the gear and on the
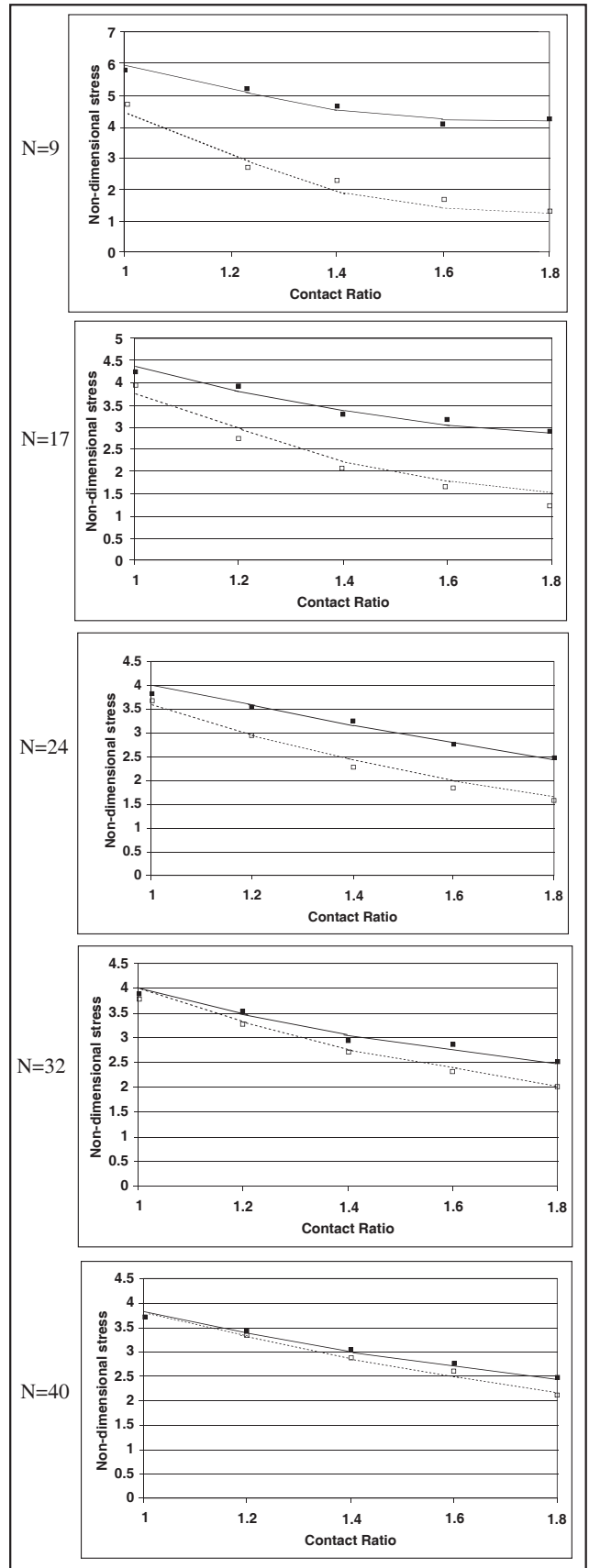
Figure 5—Non-dimensional stresses vs. contact ratio for gears with various numbers of teeth as predicted by BEM analysis and verified by photoelastic experiment. Solid line: Trochoidal fillet (BEM analysis), Solid rectangle: Trochoidal fillet (experiment), Dotted line: Circular fillet (BEM analysis), Hollow rectangle: Circular fillet (experiment).

contact ratio of the pair, the analysis results can be plotted in the form of non-dimensional stress versus contact ratio diagrams. Module- and loading level-specific results can be extracted for any given choice of parameters by use of Equation 6.

Photoelastic investigation confirmed the validity of the BEM results. Maximum deviation was less than 5%, which is deemed satisfactory. A superposition of the analytical and the experimental results is presented in Figure 5 and shows good agreement between the two. The effect of contact ratio was modelled in the experiments by displacing the position and angle of load application to correspond to the actual displacement of the HPSTC in each case.

An additional simulation was carried out where all gears were examined for interference during meshing. It was verified that no interference occurs when replacing the standard trochoidal fillet with the novel circular fillet, making the solutions geometrically and kinematically interchangeable without any restraint.

Figure 6 presents a summary of the obtained increase in load carrying capacity (decrease of maximum fillet stress) as calculated by the BEM calculations. The trend is quite clear and systematical. At N = 9 teeth, the trochoidal solution is at a severe disadvantage because of the undercutting and normally such gears are never produced. Use of the circular fillet allows for use of such otherwise prohibitively low tooth numbers in addition to its overall benefit of increasing load carrying capacity.

It is noted that the working tooth profiles remain identical in standard trochoidal and in circular fillet teeth, so no change in contact pressure takes place when switching to a circular fillet design. Circular fillets purely increase bending strength.

Overall, the new circular fillet design fares better than the standard trochoidal fillet design, especially in cases of pinions with small tooth numbers. With larger tooth numbers, the difference between the two designs becomes smaller and tends to be asymptotically zero when the number of teeth tends to infinity, as in the case of a rack, where even the standard design gives a circular fillet.

The proposed fillet geometry can be cut on conventional hobbing machines or rack-cutting machines without the need of special tooth number-specific milling tools. The generating rack need only deviate slightly from the standard rack, as its tip must be of an appropriate shape to generate the root fillet of the tooth. This generating process is simulated in Figure 7.

As it is usually pinions that undergo the higher bending stresses developed in the gear pair during meshing, the same generating rack can be used to cut the mating wheel teeth, although their root fillet geometry will not be strictly circular as for the pinion. Still, initial trials performed by the authors suggest that wheel teeth produced in this way will also exhibit increased strength compared to the conventional teeth generated with the standard circular tipped rack/hob.

Conclusion

A new circular fillet tooth design was proposed to replace the standard tooth designs currently produced by hobbing and other generation processes. The design and verification process comprised a full generation, simulation and verification cycle of the new design, including design of hob cutter fillet geometry, simulation of the generation process, calculation of fillet stress and strength evaluation and comparison with standard gears using BEM, manufacture of gear tooth samples and static load carrying capacity testing of generated gears by measuring maxi-
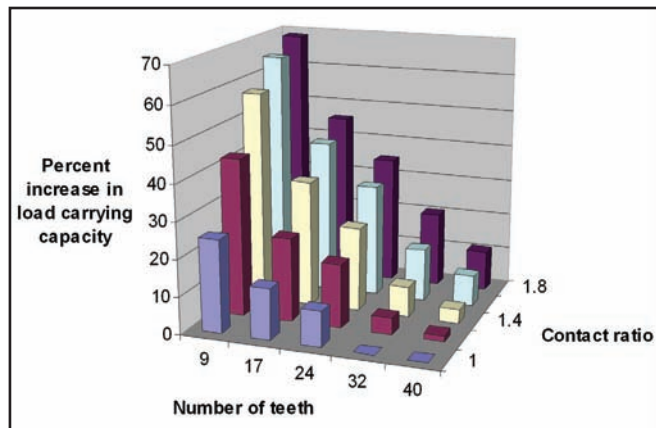
Figure 6—Calculated increase in load carrying capacity granted by circular fillet.
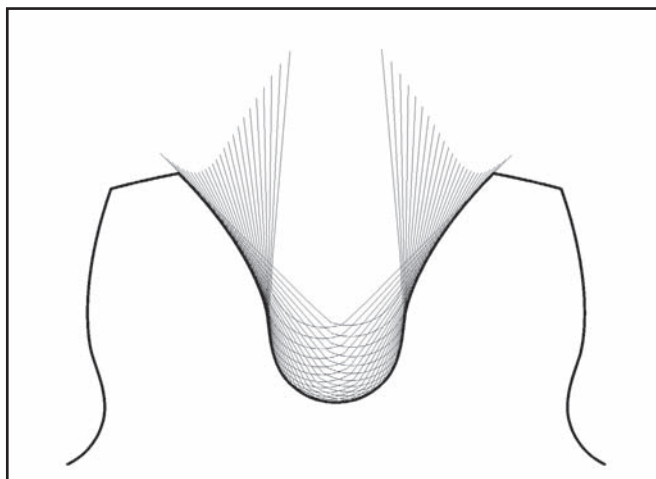
Figure 7—Schematic of the hobbing process for the production of a circular fillet.

mum fillet stress using photoelasticity.

The results show that the proposed solution achieves superior performance, especially at small tooth numbers, where undercutting otherwise becomes a serious issue, while maintaining full interchangeability with the current trochoidal fillet designs. In particular, no change is made on the involute working profile itself, so mesh kinematics and contact stresses (pitting resistance) are not affected at all.

The new design inherently dispenses with the undercutting problems that hinder the use of low tooth numbers (typically less than 17) and can be easily manufactured using standard involute hobbing tools with special tip design. The shape of the required modified hobbing tools was calculated and the generation process was shown to be no more complicated or demanding than that used currently for the production of standard gears. ⭕

References
1. Townsend, D.P. *Dudley's Gear Handbook – the design, manufacture and application of gears*, New York, McGraw-Hill, 1992.

2. Niemann, G. *Maschinenelemente*, Vol. 2, Berlin, Springer-Verlag, 1965.

3. Fredette, L., and M. Brown. "Gear Stress Reduction Using Internal Stress Relief Features," *Journal of Mechanical Design*, Vol. 119, No. 4, 1997, pp. 518–521.

4. Ciavarella, M., and G. Demelio. "Numerical Methods for the Optimization of Specific Sliding, Stress Concentration and Fatigue Life of Gears," *International Journal of Fatigue*, Vol. 21, No. 5, May 1999, pp. 465–474.

5. International Standards Organization, *ISO 6336-3: Calculation of the load capacity of spur and helical gears-Part 3: Calculation of tooth bending strength,* Geneva, Switzerland, International Standards Organization, 1996.

6. American Gear Manufacturers Association, *AGMA 2101-C95: Fundamental rating factors and calculation methods for involute spur and helical gears* (Metric version), American Gear Manufacturers Association, Alexandria, VA, 1995.

7. Mabie, H.H., C.A. Rogers and C.F. Reinholtz. "Design of Nonstandard Spur Gears Cut by a Hob," *Mechanism and Machine Theory*, Vol. 25, No. 6, 1990, pp. 635–644.

8. Rogers, C.A., H.H. Mabie and C.F. Reinholtz. "Design of Spur Gears Generated with Pinion Cutters," *Mechanism and Machine Theory*, Vol. 25, No. 6, 1990, pp. 623–634.

9. Litvin, F.L., L. Qiming, and A.L. Kapelvich. "Asymmetric Modified Spur Gear Drives: Reduction of Noise, Localization of Contact, Simulation of Meshing and Stress Analysis," *Computer Methods in Applied Mechanics and Engineering*, Vol. 188, Nos. 1–3, 2000, pp. 363–390.

10. Tsai, M., and Y. Tsai. "Design of High Contact Ratio Spur Gears Using Quadratic Parametric Tooth Profiles," *Mechanism and Machine Theory*, Vol. 33, No. 5, 1998, pp. 551–564.

11. Spitas, V.A., T. Costopoulos and C.A. Spitas. "Fast modeling of bending stresses in non-dimensional gear teeth using BEM," *Proceedings of the IASTED International Conference on Applied Simulation and Modeling*, Heraklion, Greece, June 2002, pp. 41–46.

12. Spitas, V.A., T. Costopoulos. "New Concepts in Numerical Modeling and Calculation of the Maximum Root Stress in Spur Gears versus Standard Methods: A Comparative Study," *Proceedings of the 1st National Conference on Recent Advances in Mechanical Engineering*, ASME-Greek Section, Patras, Greece, September 2001.